Tortuosity of the porous structure of carbon gels

Samantha L. Flores-López, Luis A. Ramírez-Montoya, M. Dolores Casal, Miguel A. Montes-Morán, J. Angel Menéndez, Ana Arenillas*

Instituto de Ciencia y Tecnología del Carbono, INCAR-CSIC. Francisco Pintado Fe, 26. 33011 Oviedo, Spain

* Corresponding author phone: +34 985119090. E-mail: ana.arenillas@csic.es (A. Arenillas)

ABSTRACT

Extensive studies on the correlation between synthesis variables and the final properties of resorcinol-formaldehyde carbon gels have been performed. This knowledge allows us to obtain carbon gels with analogous mean pore sizes and porosity from different combinations of synthesis variables. However, although the materials exhibit these similar characteristics, their behaviors may be very different in certain applications. Since the distribution and connectivity of the polymeric clusters are strongly affected by variables such as the amount of water and methanol in the precursor solution, it seems that the pore tortuosity and thus the permeability of the materials are also dependent on these factors. Further analysis of a series of carbon gels with the apparent same porosity shows how an increase in the amount of water or a suitable combination of methanol content and the pH of the precursor solution used for the polymerization process generate less tortuous pore structures. This allows us to attain even finer tuning of the porous structure of RF carbon gels either to reduce pressure drop or to increase the residence time of solutes in separation processes.

Keywords: Carbon gels, Mean pore size, Porosity, Permeability, Tortuosity

1. Introduction

Carbon gels are porous materials obtained by carbonization of organic polymers synthesized by sol-gel reaction of hydroxylated benzene and aldehyde (i.e. resorcinol (R) and formaldehyde (F)). The potential applications of these materials in catalysis, energy storage, adsorption, gas storage, and coatings, among other things, are as extensive as the possibilities for them to be designed to order [1–5]. In other words, one of the most valued features of these kinds of materials is the capacity to control their final three-dimensional polymeric network using the polymerization process. Thus, usually by varying the amount of solvent and/or reactants (i.e. R/F ratio, dilution ratio D, methanol content) and the pH of the precursor solution, carbon gels with different porous properties can be produced [6–9]. Moreover, different combinations of these variables may be used to obtain similar mean pore sizes in the final carbon gel.

Although variation of these porous characteristics is fundamental in improving the performance of the RF carbon gels in different applications; most of the characterization studies for these kinds of materials only report pore parameters such as mean pore size, percentage of porosity and pore volume. However, applications which involve mechanical, thermal and electrical properties are strongly related to diffusion and effective-void space. This is why a more complete characterization of porous materials has been performed in some fields, including the physical properties of the pore space, such as permeability and tortuosity [5,10–12].

Because they have a direct relationship to many applications, permeability measurements are commonly used and there are many models for producing them. Calculations based on Darcy and Poiseuille laws are widely used for experimental determinations of permeability [13–15]. However, there are few studies about RF carbon gels. Among them, the study by Kong et.al. [16] stands out, since in addition to

the experimental evaluation of the gas permeability of some RF carbon aerogels (using N_2 and Darcy´s law), the study correlated this property with density and average pore diameter by a power law relationship.

In a similar way, in addition to the different experimental methods for the calculation of permeability, a series of theories and models have been proposed in order to determine permeability and tortuosity parameters[5,13,17–21].These models are based on theories such as percolation, effective media, and fractals, each with its particular limitations and applicability. The objective of these theories is to best represent the pore structure and the microscopic properties of the pore network, including connectivity, void-space random distribution, isotropy/anisotropy, etc. The models derived from the theories try to correlate these structural characteristics with parameters related to physical properties such as conduction and mass transport. Even though percolation and effective media theories were developed many decades ago to model random media without spatial correlation, they are still considered robust and effective when are applied in empirical or semi-empirical models. However, the description of the porous structure from the statistical geometrical self-similarities of fractal theory reduces the need for empirical constants, giving it a clear superiority in estimating permeability for low permeable porous media [22,23].

Regardless of the theoretical basis, some efforts to contribute to measuring these physical parameters are based on current experimental analysis of porous media, increasing the information extracted from existing, easily obtainable data [13,14,24]. Such is the case of mercury porosimetry, a useful technique due to its simplicity and wide range of applicability which has been successfully used in simulated diffusion and conduction processes in the pore space [24–26]. From this simulation and application of

mathematical models, physical parameters (i.e. permeability and tortuosity factor) can be calculated.

Despite differences between semi-empirical and fractal models, the correct selection of parameters and considerations to correlate absolute permeability with intrinsic parameters of porous materials (i.e. pore size and pore-throat size) have produced values in good agreement with experimental measurements [27].

However, in terms of practicality, some methods have demonstrated less requirement for calculation. This is the case with the proposal from Katz and Thompson (KT) [28], an expression based on the characterization of pore space through mercury porosimetry data. Originally designed for sedimentary rocks, use of the KT equation has extended to shales, claystones, cement and graphite, showing excellent correlation with experimental data [29–31]. However, in the analysis of coals, KT values showed variations by orders of magnitude, although they did allow comparative analysis by maintaining the same behavior as the experimental permeabilities [32]. In order to predict the absolute permeability of porous solids, this model uses intrusion data to determine characteristic diffusion lengths and paths (see Figure 1), values used in the KT equation as follows:

$$k = \left(\frac{1}{89}\right)(L_{max})^2 \left(\frac{L_{max}}{L_c}\right) \emptyset S(L_{max}) \quad (1)$$

Where L_c and L_{max} correspond to the characteristic and maximum diffusion lengths respectively, $\emptyset$ is the porosity fraction and $S(L_{max})$ is the interconnected volume fraction with pore diameter greater than or equal to L_{max} [15,25,26,28]. One of the robust characteristics of this model is that different authors have produced new values for the constant (1/89 for hydraulic conductance in pores with a constant length), adapting it to the type of pores which describe the system[15].

a) b)

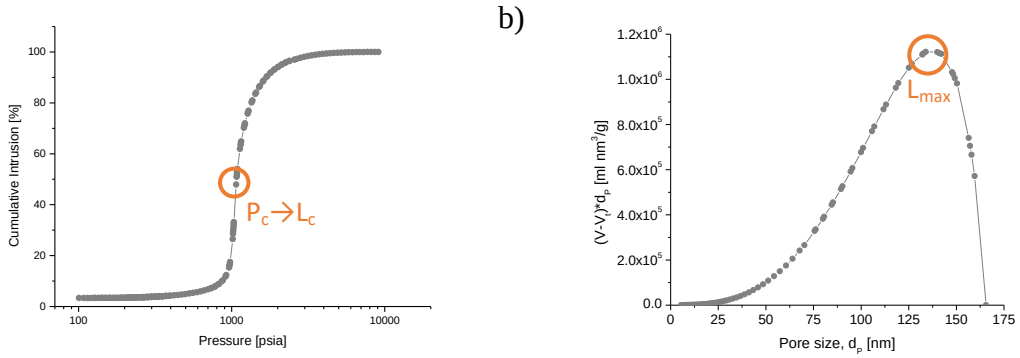

Figure 1. Graphical determination of useful length pore sizes from mercury intrusion data using the KT method. a) Characteristic length (L_c) at the threshold pressure (P_c) and b) Length of maximum diffusion (L_{max}) from diffusion path.

The tortuosity factor (τ), is a parameter that is related to the structure of the solid, and represents the difference between theoretical diffusion and measured (or effective) diffusion, including all deviations from straight diffusion paths, in a single dimensionless parameter. Unlike other models, in this case the empirical equation (Equation 1) proposed by Carniglia et. al. [33] left the tortuosity factor as an independent parameter of permeability, which is why the value obtained can be considered a consequence of network structure. This characteristic makes the Carniglia tortuosity factor a good reference parameter to compare with permeability results or different kinds of tortuosity (such as hydraulic tortuosity). Based on Fick's first law and assuming a uniform, isotropic material, Carniglia's expression is as follows:

$$\tau = 2.23 - (1.13 V_{Hg} \rho_b) \quad (2)$$

Where V_{Hg} corresponds to the total specific pore volume (determined by mercury volume intruded at maximum experimental pressure) and ρ_b corresponds to the bulk density. The product of the two corresponds to the material porosity (P) with its value lying between 0.05-0.95. The constant values of Equation 2 come from the linear equation obtained by mathematical treatment of diffusion behavior and its relationship

with pore dimensions (i.e. radius and length), tortuosity, and porosity. This correlation by Carniglia for catalyst with cylindrical pores and any pore size distributions presumed to be generally applicable. However, considerable differences were noted compared to experimental values and a more generalized form including non-cylindrical diffusion paths was constructed:

$$\tau = \left[2.23 - \left(1.13 V_{Hg} \rho_b\right)\right](0.92y)^{1+\varepsilon} \quad (3)$$

Where $y = \frac{S_{Hg}}{S_{BET}}$ (4)

This extension of equation 2 was obtained through the mathematical treatment of the mass transport rate of cylindrical and non-cylindrical paths, assuming bulk and ideal Knudsen diffusion. In both cases, the ratio of mass transport has comparably linear behavior. Hence Equation 3 includes the constant slope of this linear model (i.e. 0.92) and the pore shape factors *y* and ε. Factor *y* is defined as the ratio between the surface area determined by mercury porosimetry (S_{Hg}) and the surface area from the BET equation (S_{BET}) (see Equation 4). When y is lower than 1.1, the simple form of the Carniglia equation (Equation 2) can be used. The shape factor exponent, ε, is determined experimentally through the diffusion path and takes values between 0 and 1. Tortuosity values are usually between 1 and 7, and are usually close to 2 for non-intersecting cylindrical pores, and greater than 2 when non-cylindrical pores are prevalent in the material [14,24].

Unlike other studies with porous carbons, where the aim is to confirm the correlations established between the porous and physical parameters such as tortuosity and permeability [17,34–36], in this study values of permeability and tortuosity are determined from mercury intrusion data with models currently known to be robust

[15,34,37]. In this way it is possible to increase the existing information about these physical parameters in RF carbon gels without the need for additional analysis.

Additionally, the present study focuses on the comparative analysis of permeability and tortuosity parameters between RF carbon gels which had previously been considered analogous due to their similar average pore sizes. The detailed characterization of the porous structures of the selected samples allows us to correlate their structural differences with the different values of tortuosity and permeability, thus increasing knowledge about the design of these kinds of materials and their viability in many applications.

2. Experimental procedure

2.1 Synthesis and characterization of carbon gels

Organic gels were obtained from a sol-gel process on the basis of precursor solutions of resorcinol (R, Indspec 99%)-formaldehyde (F, Merck 37 wt.% water, 10 wt.% methanol content), using methanol (AnalaR NORMAPUR ©, 99.9 %) to increase the percentage in the formaldehyde solution, water as a solvent and NaOH and HNO_3 as catalysts. In order to control the porous structure and to obtain similar mean pore sizes in the final RF gel, the solutions used included different combinations of synthesis variables such as R/F ratio, dilution ratio D which means the ratio of the total solvents used (water and methanol) with monomers (R and F), methanol content in the F solution and pH of the final precursor mixture, shown in Table 1. According to previous research, decreasing the pH of the precursor solution produces RF gels with wider pores, and decreasing the dilution of the initial mixture would lead to narrower pores [7,9,38]. Therefore, a proper combination of these two variables would lead to materials with similar pore sizes (i.e.

samples CX-100 and CX-100T). A similar strategy was employed by varying the pH and the amount of methanol in the precursor solution, as higher amounts of the latter would lead to RF gels with narrower pores [8] (see samples CX-45, CX-45T, CX-160,CX-160T, CX-1600 and CX-1600T in Table 1).

Adjustment of the synthesis variables was done following the methodology previously reported by Alonso-Buenaposada et.al. [8]. The precursor mixture with the defined R/F ratio, D ratio (taking into account the water and methanol present in the mixture), the methanol content in the F solution (note that an increase of the methanol content would imply less water adder for a constant D ratio), and pH defined in Table 1 is polymerized by a sol-gel process (i.e. polymerization, curing and drying steps) under microwave heating lasting just 5 hours [39]. The RF gels obtained were carbonized at 1000ºC under N_2 flow (150 ml/min) in order to obtain the carbon gels. These carbon gels were obtained as monoliths, although for some of the characterization they were crushed and sieved. Samples were denoted as CX followed by a number indicating mean pore size and, depending on the tortuosity value, a "T" suffix for the most tortuous sample (see Table 1).

Table 1. Synthesis variables used for precursor solutions

Sample	R/F	D	MeOH* [%]	pH
CX-45T	0.6	4.6	10	5.1
CX-45	0.6	4.6	13	4.5
CX-100T	0.5	5.6	10	4.5
CX-100	0.5	7.7	10	5.5
CX-160T	0.5	5.6	10	3.8
CX-160	0.5	5.6	13	3.5
CX-1600T	0.5	5.6	13	2.7
CX-1600	0.5	5.6	10	3.1

*MeOH content in the formaldehyde solution used

Similarity between the mean pore sizes (d_p) of each pair was confirmed with mercury porosimetry (AutoPore IV Micromeritics). Before porous characterization, all samples were crushed and sieved to obtain particles with a size between 2-3 mm and outgassed under vacuum at 120ºC overnight. From the same analysis, pore properties such as total intruded volume (V_{Hg}), mesopore (V_{meso}, <50nm) and macropore (V_{macro}, >50nm) volumes were obtained.

Porosity (P) and total pore volume (V_P) of the carbon gels were determined from the correlations between helium ($\rho_{He,}$ AccuPyc 1330) and envelopment density ($\rho_{env,}$ GeoPyc1360) as follows:

$$P(\%) = \left(1 - \frac{\rho_{Env}}{\rho_{He}}\right) 100 \quad [5]$$

$$V_P = \left(\frac{1}{\rho_{Env}} - \frac{1}{\rho_{He}}\right) \quad [6]$$

BET surface area (S_{BET}) and micropore volume (V_{microt}) were determined by N_2 adsorption-desorption isotherms at 77K (Tristar II from Micromeritics) using BET and t-plot models, respectively. Finally, the carbonaceous morphology was also characterized by SEM, using cross-sections of resin-embedded carbon gels for better visualization of the pore channels.

A Lab RAM HR 800 Horiba Jobin Yvon Raman spectrometer equipped with a green laser (λ = 532 nm) and a CCD detector was used for structural analysis of the materials. The laser was focused on the samples using an optical microscope (BXFM, from Olympus; 100x objective lenses) rendering an incident beam of ca. 2 μm in diameter. Raman signal was collected using a 180º geometry and a1800 lines mm^{-1} grating was used to split the incoming radiation, the spatial resolution of the Raman measurements being 0.3 cm^{-1}. Typical exposure times of 30 s were used in each of three consecutive

spectrum acquisitions. For a given sample, Raman spectra were obtained from at least three different locations. Raman signals were fitted to two lorentzian bands after a linear background subtraction.

2.2 Determination of physical parameters: Permeability and tortuosity

Values for permeability and tortuosity factors were obtained via the methods proposed by Carniglia [33] and Katz-Thompson [28] using the mercury intrusion data for each sample. In the case of Carniglia tortuosity (τ_c), all sample values were calculated using the original form of the tortuosity equation (Equation 2) due to the "*y*" factor being less than 1.1 for the full series evaluated in this study. This meant it was not necessary to use the expanded Carniglia equation (Equation 3). The characteristic length (L_c), length of maximum diffusion (L_{max}), and absolute permeability (k_{KT}) were determined by evaluation of the diffusion path and the KT equation (see Figure 1 and Equation 1).

In order to have comparative values, two software packages were used as alternative sources for these parameters. One was MicroActive from Micromeritics ©: Porosimetry data and the calculated values of characteristic length were used as the input to produce a tortuosityf actor (τ_{MA}) and permeability (k_{MA}) for all samples. In this case, a version of the Katz and Thompson equation based on the conductivity formation factor was used to determine permeability, while the tortuosity factor was determined from the permeability (applying the Hager equation [5,40]) and a constriction factor (i.e., ratio of cross-sectional areas) [25].

In addition, PoreXpert software was used to construct a unit cell on the basis of the mercury intrusion data. The unit cell with the best fit was chosen to analyze tortuosity (τ_{pX}) and helium and water permeability at 1 atm and 25 ^{o}C ($k_{HepX,}$ k_W). In this case, the

measurement of tortuosity was made directly from the relative path length calculated from the unit cell.

In order to compare the theoretical values of permeability, described above, with experimental data, a series of experiments of helium permeability were carried out at constant temperature and pressure conditions (i.e., 25 ^{o}C, 1 atm). Helium flow was circulated through a cylindrical section of the carbon gel monolith (i.e. diameter 1 cm, length 0.5 cm), and the pressure drop in the flow was registered. The collected data were then used in Equation 7, a modified version of Darcy´s law described by Springer et. al [41] for air permeability:

$$k = Q\left\{\frac{2\mu L}{A}\frac{P_0}{{P_i}^2-{P_0}^2}\right\} \quad [7]$$

where k is the permeability, Q is the He flow, A is the cross-section area, L the length of the piece, μ the He viscosity, and P_i/P_o are the inlet/outlet pressures. Creating a graph of Q against k, the data show a straight line, the y-axis intercept of which corresponds to the experimental value for absolute permeability (k_{HeE}).

3. Results and discussion

3.1 RF carbon gels and their porous characterization

Samples with four different pore sizes were obtained by a combination of the synthesis variables given in Table 1. Figure 2 shows the Hg intrusion-extrusion plots (i.e. percent of accessible void space intruded) for the samples studied. The intruded volume increases slowly at low pressures, but once the pressure reaches a certain value, the intrusion increases sharply, ending again with a smooth increase. As Figure 2 shows, the pressure at which this considerable increase in intrusion is obtained overlaps for

each pair of samples, and as a consequence, they have a similar mean pore size value (see Figure S1, Supplementary Information). A displacement of that sharp increase to the left can also be seen as the pore size increases (e.g. Figure 2a and 2b).

On the other hand, the extrusion curves show that nearly all the mercury is retained in the porous structure for all samples. Only the samples with wider pores (i.e. CX-100 and CX-1600) shows a small release, less of 20% of the total intruded mercury. This is due to the fact that during intrusion the pressure is increased to have an intruded volume of maximum 0.01 mL/g with an equilibrium time of 10 s, which means pressure increments between 0.001 and 0.05 MPa. These analysis conditions give the data with the enough quality to apply the different models used in this study. However, after this the analysis is considered finished and then the pressure is decrease (i.e. during the extrusion) in the order of several units of MPa, and there is not enough time for a proper release of all mercury intruded.

The mean pore sizes, along with the other pore properties produced by Hg porosimetry are presented in Table 2. The difference between d_p values (in pairs) increases as the pore size increases; however, the corresponding orders of magnitude allow us to consider these variations within experimental error. On the basis of the assigned values (i.e. 45, 100, 160 and 1600 nm), the pair with the lowest diameter could be classified as a mesoporous material (i.e. CX-45 and CX-45T), while the remaining samples are macroporous materials.

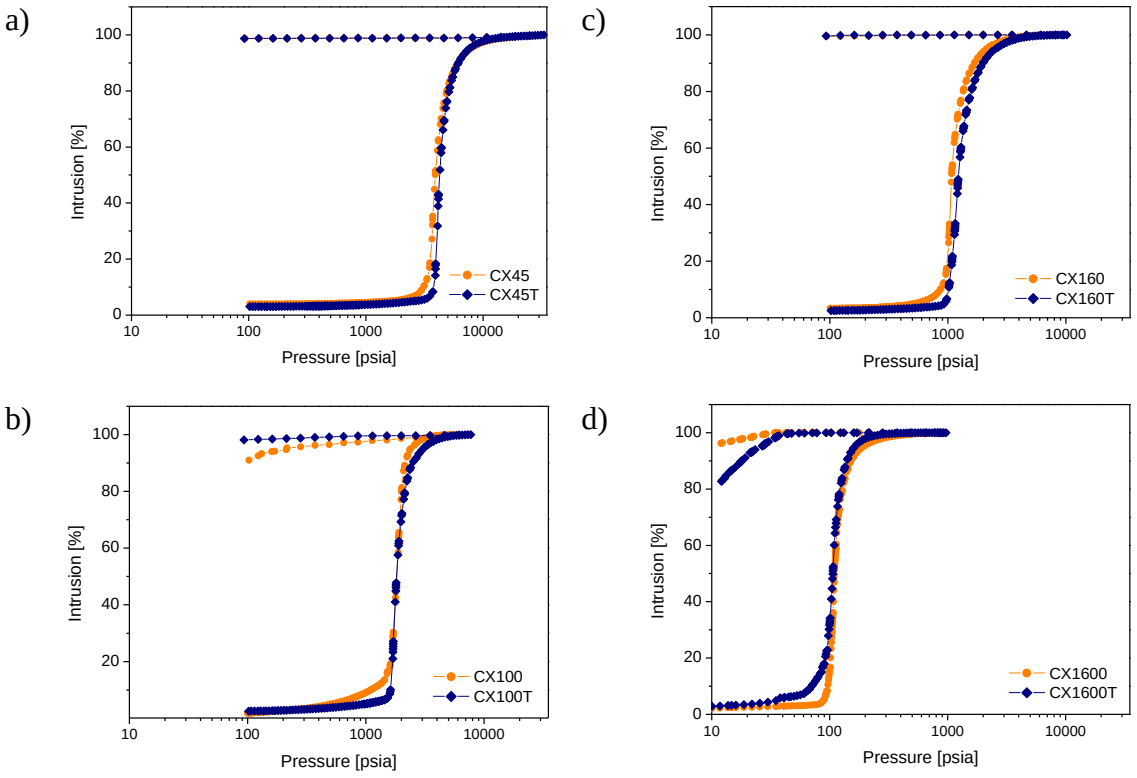

Figure 2. Hg intrusion-extrusion curves for the samples, as percent of accessible void space.

Although the samples are considered meso- and macroporous from porosimetry analysis, N_2 adsorption-desorption isotherms at 77 K were performed in order to have a complete picture of their pore characteristics. The resultant isotherms are presented in Figure 3, which shows that their shapes match in each pair across all ranges of relative pressures, indicating the presence of similar porosity at the micro- and mesopore level.

According to IUPAC classification [42], with the exception of CX-1600 and CX-1600T, the samples exhibit type II isotherms, which is characteristic of materials with wide porosity and therefore an unrestricted mono and multilayer adsorption isotherm. The sharp knee at low p/p_0 in all isotherms is due to the presence of certain microporosity which is typical of this type of materials [6,43] irrespective of their mean pore size, while the N_2 adsorption at high p/p_0 is attributed to partial filling of wide pores detected by this technique. The presence of a type H3 hysteresis loop in the isotherms from

samples CX-45 and CX-45T (Figure 3a), indicates a network with pore sizes in the upper limit of the mesoporous range. The total volume adsorbed at p/p_0=1 clearly decreases with increasing mean pore size. In fact, samples CX-1600 and CX-1600T (Figure 3d) show type I isotherms [42], where the amount of N_2 adsorbed approaches a limiting value controlled by the accessible micropore volume. However, this clearly does not mean a decrease in porosity but rather that this technique (i.e. N_2 adsorption isotherms) does not properly characterize the wide pores in macroporous samples.

Each pair of samples exhibited similar micropore volumes and thus analogous BET surface areas (see Table 2), around the expected values for these types of polymeric materials. Helium densities show small variations due to the R/F ratio and the catalyst used, whilst envelopment densities give different values as a consequence of the increase of pore size for the complete series. Helium densities give values between 1.65-1.82 g/cm^3, while envelopment density values vary between 0.27-0.53 g/cm^3. The percentages of porosity calculated from density values are not very different (i.e. between 70 and 80%) although there are samples with large variations in mean pore size (from 45 to 1600 nm). In this regard, the total pore volume (V_P) does show a variation, even between the pairs with similar pore sizes (e.g. 2.09 and 3.04 cm^3/g for samples CX-1600T and 1600).

a)

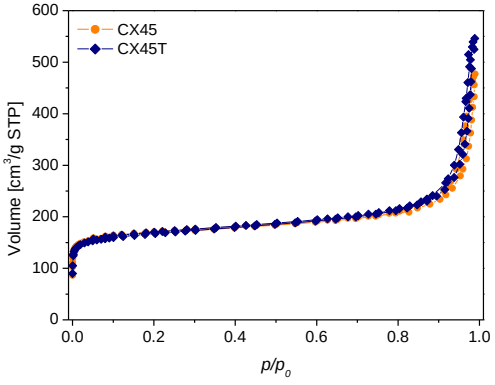

c)

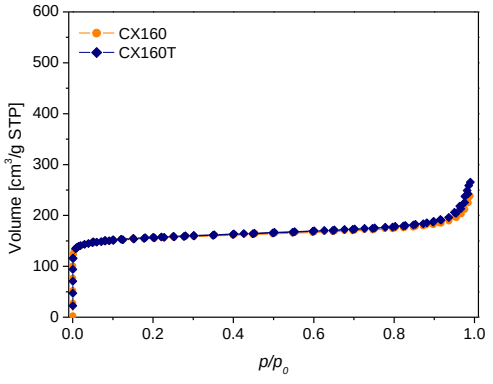

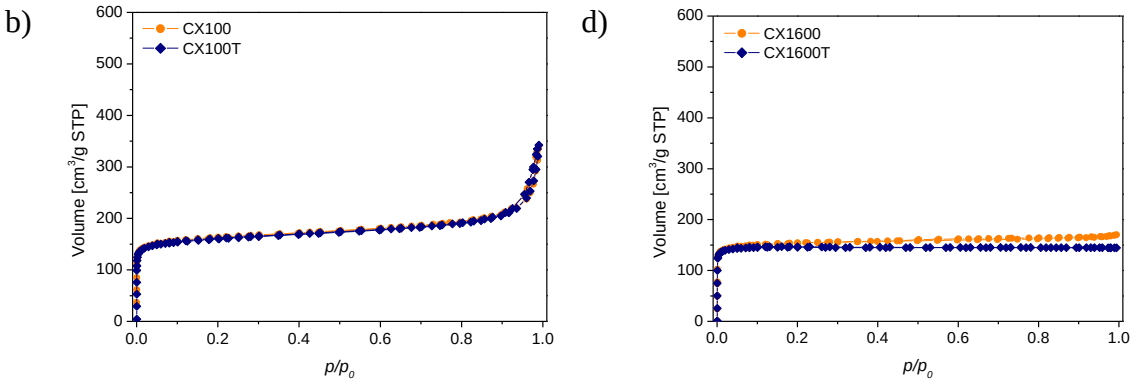

Figure 3. N_2 adsorption-desorption isotherms at 77 K.

Table 2. Porous characterization of RF carbon gels.

Sample	d_p	ρ_{He}	ρ_{env}	Porosity	V_P	V_{Hg}	V_{macro}	V_{meso}	$V_{micro\ t}$	S_{BET}
	(nm)	(g/cm^3)	(g/cm^3)	%	(cm^3/g)	(cm^3/g)	(cm^3/g)	(cm^3/g)	(cm^3/g)	(m^2/g)
CX-45T	43	1.82	0.48	73	1.51	1.21	0.10	1.11	0.18	630
CX-45	46	1.78	0.53	70	1.34	1.07	0.28	0.79	0.19	643
CX-100T	101	1.76	0.36	80	2.23	1.70	1.67	0.03	0.19	620
CX-100	99	1.76	0.31	82	2.65	2.36	2.32	0.04	0.19	627
CX-160T	152	1.74	0.35	80	2.28	1.93	1.88	0.05	0.19	612
CX-160	168	1.68	0.36	78	2.16	1.71	1.67	0.04	0.20	610
CX-1600T	1692	1.69	0.37	78	2.09	1.69	1.67	0.02	0.23	600
CX-1600	1663	1.64	0.27	83	3.04	2.83	2.82	0.01	0.21	606

Total pore volume and total intruded volume (V_P and V_{Hg}) show natural differences due to the presence of blocked or small pores that are not accessible during Hg porosimetry. Mercury porosimetry does not characterize pores narrower than 5 nm. However, it is worth noting that both parameters follow the same trend (see Table 2). Therefore, V_{Hg} may be considered a representative parameter. In other words, Hg porosimetry characterizes the required porosity range to describe all samples correctly.

Unlike in previous studies [44–46], we compare the porous characteristics of each sample pair with a similar mean pore size, including the range of micro-, meso- and macropore volumes. In the case of CX-45 and CX-45T, although the differences in total intruded volume (V_{Hg}) are not large, the respective contribution of the meso- and macropore volumes is different. In the remaining samples, variations in total intruded volume (V_{Hg}) are directly related to variations in macropore volume.

In the case of carbon RF gels, the formation of these porosities is a consequence of the size of the polymeric clusters, and those are defined by the synthesis variables. For samples CX-100 and CX-100T, in addition to varying the pH of the precursor solution, the dilution ratio was also varied (i.e. 5.6 and 7.7, see Table 1). As noted above, the aim of this study was to modify these two variables in order to obtain samples with analogous mean pore sizes, and Table 2 shows that this was successfully achieved. However, this combination also affects the structure of the polymeric network (i.e. crosslinks between clusters). An excess of water in the precursor solution clearly has an influence on the reaction between the diluted precursors, in some way minimizing the crosslinking reactions between clusters. Therefore, although the mean pore size is similar, the intrinsic pore structure may not be.

Similarly, the effect of methanol content on pore properties has previously been studied. Alonso-Buenaposada et. al. reported that higher pore volumes were obtained for the full range of pH (2-7) when the content of methanol decreased, and this effect seems to be more pronounced at lower pH [8,47]. This behavior is related to interactions between methanol and formaldehyde, since formaldehyde's participation during polymerization is inhibited by the presence of methanol. It is believed that the reactions involving formaldehyde are crucial in the reinforcement of the polymeric structure by some crosslinking reactions. Therefore, increasing the methanol content inhibits those reactions and leads to a weaker polymeric structure that may partially shrink during the drying step, producing samples with lower pore volumes. However, even with the effects of this collapse, a structure with more complicated access cavities can be produced by reducing the amounts of MeOH.

Although the variation of these parameters (i.e. pH, dilution and methanol content) affects properties such as pore volume, pore shape and connectivity, at the

microstructure level they do not cause any alteration. To confirm this, Figure 4 shows the Raman spectra of different carbon gels. Essentially, the Raman profiles are identical regardless the pore size of the samples (Figure 4a) or between pairs with a given pore size (Figure 4b). They all are typical spectra of highly disordered carbons, with the D and G bands merged. Calculation of the I_D/I_T (%) parameter confirmed the absence of significant differences in the structural order of all carbons in the study (See Figure S2 in Supplementary information), i.e., their microstructure remains comparable in all cases.

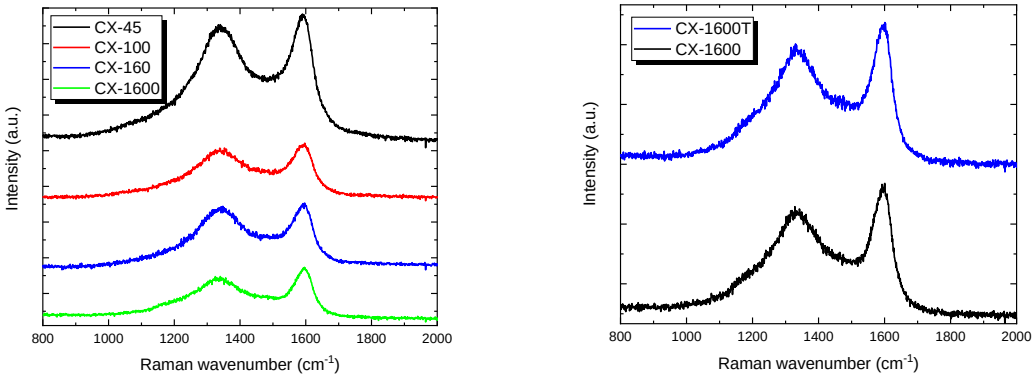

Figure 4.a) Raman spectra of CXs with different pore size; b) Raman spectra of a pair with similar pore size

In addition, Figure S3 in supplementary information shows the macroscopic appearance of the samples, evidencing their apparent similarity.

3.2 Physical parameters: Tortuosity and permeability

As described in the experimental section, mercury porosimetry data were used to determine values for tortuosity and permeability. The diffusion paths produced during the data treatment with the Katz and Thompson model (KT) are presented in supplementary information (see Figure S4). As expected, the characteristic lengths (*Lc*) obtained from the databases and reported in Table 3 are practically the same as the

mean pore sizes. Since they were calculated with the same model, permeability from KT (k_{KT}) and MicroActive software (k_{MA}) had only slight differences in their values (see Table 3). In all cases, both permeabilities show small but noticeable differences between pairs of carbon gels with similar pore sizes. In addition, if we compare between groups (e.g. group CX-45 against group CX-100), these permeability values follow a logical incremental trend with increasing pore size. It is also notable that permeability increases by one or two orders of magnitude when the mean pore size is two or 10 times larger, respectively. The k_{KT} and k_{MA} parameters correspond to absolute permeabilities as both come from variants of the KT model.

PoreXpert simulations were carried out with all available models to find the best fit for the data. The existing models are classified in four groups: random, horizontal banded, vertical banded, or spherical, depending on the characteristic arrangement of the network [37]. The vertical model relates to networks with pores and throats of similar sizes arranged as vertical bands, while the spherical model considers a central spherical zone with a different pore size from the surrounding area. In contrast, horizontal banded models are usually correlated with materials based on distinct layers arranged as horizontal bands or woven structures with a broad pore size distribution. These pore sizes can be ordered from large-to-small or small-to-large from the surface, and both arrangements are considered in the model.

The chosen models (see Table 3) were run with five different initial stochastic generations per sample in order to obtain an average of the calculated data. It is worth noting that all samples studied exhibited a better fit with random or horizontal models (i.e. large-to-small and small-to-large), which makes sense considering the fact that our materials do not have cores with variable density and usually present constrictions (i.e.

throat sizes that are different from pore sizes). Figure S5 in Supplementary information shows the fit of the selected models given in Table 3.

The behavior of the permeability values from the PoreXpert simulation, k_{HepX} and k_W, is in good agreement with the trend shown by the absolute permeabilities, despite being calculated for a specific fluid (i.e. taking into account the mean free path of helium and water). Helium permeability values (k_{HepX}) are in the same order of magnitude as k_{KT} permeabilities, whilst water permeability (k_W) presents lower values, which is expected due to the nature of the fluids and the conditions of evaluation (i.e. 25ºC, 1atm).

Finally, the experimental values of helium permeabilities (k_{HeE}) exhibit the same trend as the theoretical values. Although the experimental and simulated operating conditions were the same (25ºC, 1atm), variations in orders of magnitude were registered (see Table 3). Based on other reports with coals and sandstone rock, variations between two and four orders of magnitude are considered acceptable in these cases due to the nature of the methodology used for the calculation [30,32]. Experimental helium permeabilities can be greater than simulated permeabilities because the sample piece used during determinations contains pores of multiple sizes, combining Knudsen diffusion and Darcy´s permeability in the results produced [17,48–51]. The contribution of small pores playing a throat role between larger pores also has a significant effect on the flow rate [52]. In addition, consideration of scaling factors referring to experimental conditions (i.e. sample dimensions), interactions with nanoparticles, and existing micro fissures also have considerable influence on the magnitude of the experimental results.

There are few reports about experimental helium permeability in porous materials, they include the evaluation of cores from Eagle Ford shales (mineral-carbon material) with approximately 2 nm of mean pore size, using pulse decay techniques, resulting in a permeability of 0.04 mD [48]. Moreover, the order of the experimental permeabilities in

this study agrees with other values reported for RF materials. RF aerogels with bulk densities of 0.05-0.45 g/cm^3 and mean pore sizes between 5-26 nm present N_2 permeabilities around 0.32-8.6 mD [16], whilst permeability results for diverse carbon materials (e.g. fibers, foams and felts) with high porosity and pore diameters of microns, are always above 10 Darcy [11,53,54]. The characteristics of the samples in the present study may be considered in the middle of those described in the mentioned studies.

Table 3. Permeability parameters and tortuosity factors for the carbon gels studied.

Sample	Lc[nm]	Permeability [mD]					Tortuosity			Model
		k_{KT}	k_{MA}	k_{HeE}	k_{HepX}	k_W	τ_c	τ_{MA}	τ_{pX}	pX
CX-45T	42	0.41[a]	0.22[a]	24.62	0.04[a]	-	1.54	1.87	1.65	Small to large
CX-45	46	0.42[a]	0.27[a]	34.96	0.06[a]	-	1.57	1.85	1.56	Random
CX-100T	100	2.58[a]	1.95[a]	27.16	1.08[a]	0.06[a]	1.54	1.76	1.57	Random
CX-100	96	3.74[a]	2.51[a]	48.53	2.95[a]	0.18[a]	1.40	1.72	1.28	Large to small
CX-160T	150	3.95[a]	2.59[a]	548.17	3.71[a]	0.30[a]	1.42	1.80	1.46	Random
CX-160	166	5.99[a]	4.17[a]	735.62	6.93[a]	0.64[a]	1.46	1.78	1.35	Small to large
CX-1600T	1691	7.90	5.39	17022.6	0.92	0.49	1.49	1.79	1.33	Large to small
CX-1600	1657	9.00	5.59	23507.4	1.54	0.76	1.36	1.72	1.22	Random

[a]Divided by 10^{-2}

In addition, the tortuosity values are interesting. Since lower tortuosity means more available routes to cross a section of material, it is assumed that samples with the highest permeability will be less tortuous. And this is the case when comparing the tortuosities against permeability values, regardless of the methodology used for the calculation. The variation by pairs of the MicroActive tortuosities (τ_{MA}) depends on their permeability values, resulting in close values that follow the expected trend for the complete series. However, Carniglia's tortuosities (τ_C) present an incomplete description of the connectivity in the porous solids, reflecting behavior related only to bulk density and pore volume values of Hg porosimetry [55]. Therefore, these values of tortuosity will reflect differences as large as the differences between these parameters. Finally, the statistic used in the calculation of tortuosity from a simulation (τ_{pX}) seems to yield

greater differentiation between the samples, even exhibiting a slight decrease with increasing pore size. However, all tortuosity values reported in this study are in good agreement with previously reported values. Based on the Carniglia equation, Seifi et. al. [56] reported tortuosities between 1.12 and 1.63 for carbon gels with very similar porous properties to ours (i.e. 66-80% of porosity, around 600 m^2/g of superficial area and 0.87-3.0 cm^3/g of V_{Hg}). On the other hand, according to a study on porous carbons, hydraulic tortuosity ranges from 1.5 to 2.0 [34].

In all cases, samples from the CX-45 and CX-160 groups presented negligible differences between tortuosity values, which is why they could be considered almost identical. In contrast, the samples from the CX-100 and CX-1600 groups exhibited more evident variance.

To clarify what is happening with the samples in this study, it is important to compare physical and porous properties. First, it is essential to note that both permeability and tortuosity values are not only influenced by porosity properties, but also by the network structure (i.e. distribution of clusters, crosslinks, etc.).

When samples with similar pore sizes but bigger differences in pore volume are evaluated, the advantage of having more empty space available makes them the most permeable and unquestionably the least tortuous. Such is the case with pairs CX-100 and CX-1600 (see Table 2 and 3). Visual evidence of this phenomenon is shown in Figure 5, where c,d and g,h samples correspond to the CX-100 and CX-1600 pairs, respectively. In these SEM images, it is clear that the sample with the highest dilution ratio (i.e. CX-100, Fig. 5d) and the one with the lowest MeOH content (i.e. CX-1600, Fig. 5h) are the networks with more effective pore volume available for permeation in comparison with their correspondent counterparts. However, these notable differences in available volume were reached by different phenomena during gelation: in the CX-

100 pair, by varying the dilution ratio and creating a porous structure with more connectivity, and for the CX-1600 pair, through the variation of methanol content in an acidic pH, generating a more interconnections between clusters, and consequently, a more resistant structure to possible collapse. A noticeable effect of MeOH content can be seen by comparing Fig. 5g and 5h. The distribution of the clusters in the CX-1600T sample (Fig. 5g) is compact and creates large pores between its aggregates, unlike sample CX-1600 (Fig. 5h) whose pores are formed between the extended network generated between clusters.

In contrast, when samples with a similar pore size have small differences in pore volume, there is no notable advantage and other characteristics come into play. That is the case in pairs CX-45 and CX-160 (see Table 2 and 3), where the bigger pore volume does not necessarily lead to higher permeability and as a consequence, the tortuosity values exhibit smaller differences depending on what is considered when calculating them, and may appear to be similar. In the case of these samples, the presence of bridges or interconnections able to obstruct the pore space play an important role in the tortuosity of the samples (see magnified inlets in Figures 5a and 5e).

For example, the pore volume difference between sample CX-160 and CX-160T is around 0.2 cm^3/g and both samples appear to have the same tortuosity (see Table 3, τ_C and τ_{MA}). However, as Figure 5e and 5f (samples CX-160T and CX-160) show, due to the absence of interconnections related to the methanol content, the pores from sample CX-160 are less obstructed and therefore the sample is more permeable. The same observation applies to samples CX-45T and CX-45 (Figure 5a and 5b).

In summary, samples with analogous mean pore sizes may present different porous structures. Pore volume and the degree of crosslinking in the polymeric network may

determine the tortuosity and permeability of the samples, and therefore their behavior in possible further applications.

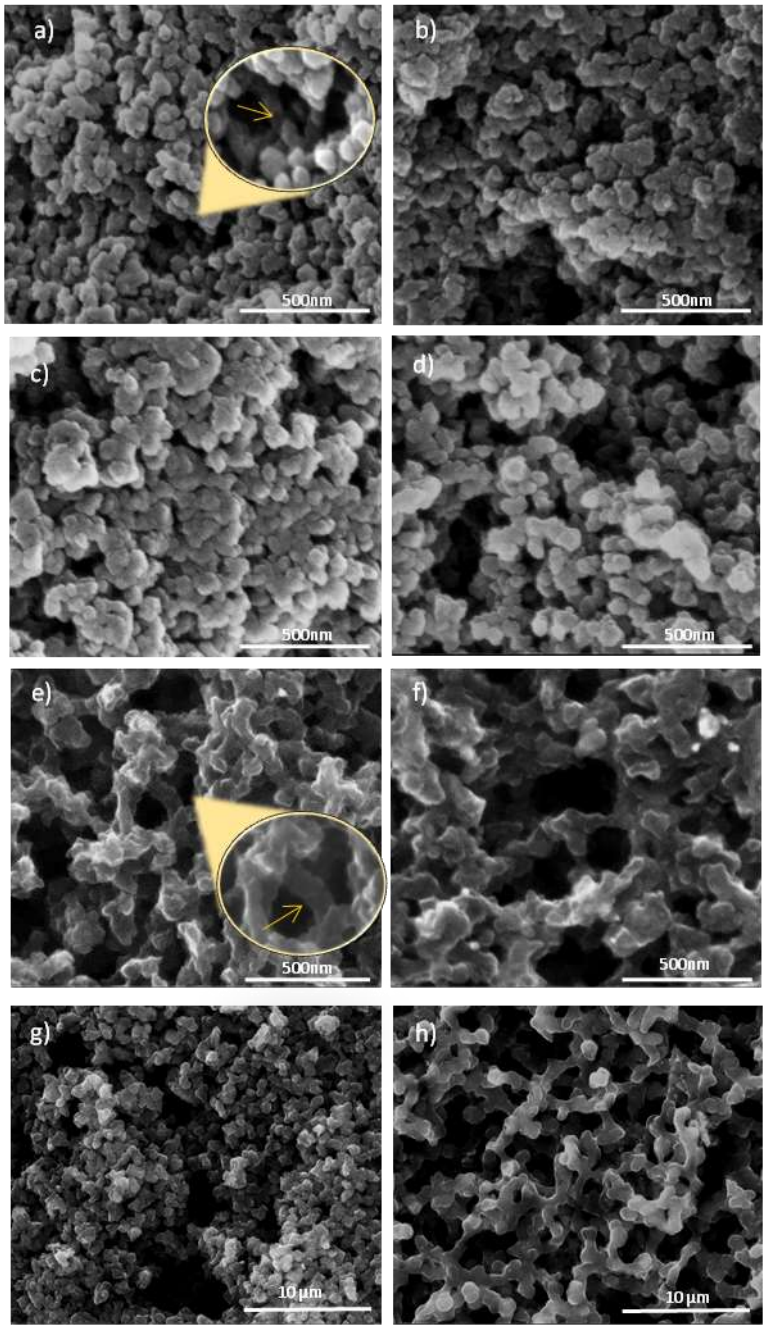

Figure 5.SEM images of cross-sections of carbon gels. a) CX-45T, b) CX-45, c) CX-100T, d) CX-100, e) CX-160T, f) CX-160, g) CX-1600T and h) CX-1600.

4. Conclusions

Different combinations of synthesis variables of RF gels (mainly the amounts of water or methanol, and the pH of the precursor solution) may lead to samples with analogous mean pore sizes. Although these samples may be thought to present similar porosity, in this study we have shown that the polymeric structure is different, affecting particularly tortuosity and permeability values.

This means that certain physical properties such as tortuosity and permeability may also be designed by modifying chemical variables during synthesis, which could be very important in subsequent applications for these materials in separation processes. Higher amounts of water in the precursor solution can lead to a better interconnected void space in the resultant gel, and consequently a less tortuous material being produced. In contrast, the effect of methanol content on tortuosity is dependent on the initial pH of the precursor solution. At a higher pH, the absence of interconnections leads to a less tortuous material (i.e. more methanol is needed). While with an acidic precursor solution, the pore volume is the key to obtaining a less tortuous material (i.e. less methanol is needed).

Acknowledgements

Authors are grateful for the financial support received from the Ministerio de Economia, Industria y Competitividad from Spain (CTQ2017-87820-R) and Principado de Asturias–FICYT-FEDER(IDI/2018/000118). SFL is grateful to the Administración del Principado de Asturias for her research training grant awarded through the "Severo Ochoa" program. LARM thanks CONACYT, Mexico for a post-doctoral grant (CVU No 330625, 2017). The authors would like to thank to Dr. Marbán for his helpful contribution with the experimental helium permeabilities.

References

[1] N. Rey-Raap, A. Arenillas, J.A. Menéndez, Carbon Gels and Their Applications: A Review of Patents, in: P. Bettotti (Ed.), Submicron Porous Materials, Springer International Publishing, Cham, 2017: pp. 25–52. https://doi.org/10.1007/978-3-319-53035-2_2.

[2] J.L. Figueiredo, Carbon gels with tuned properties for catalysis and energy storage, Journal of Sol-Gel Science and Technology. 89 (2019) 12–20. https://doi.org/10.1007/s10971-018-4633-y.

[3] J.F. Vivo-Vilches, A.F. Pérez-Cadenas, F.J. Maldonado-Hódar, F. Carrasco-Marín, C. Siquet, A.M. Ribeiro, A.F.P. Ferreira, A.E. Rodrigues, From Carbon Molecular Sieves to VOCs filters: Carbon gels with tailored porosity for hexane isomers adsorption and separation, Microporous and Mesoporous Materials. 270 (2018) 161–167. https://doi.org/10.1016/j.micromeso.2018.05.010.

[4] M. Osińska, Removal of lead(II), copper(II), cobalt(II) and nickel(II) ions from aqueous solutions using carbon gels, Journal of Sol-Gel Science and Technology. 81 (2017) 678–692. https://doi.org/10.1007/s10971-016-4256-0.

[5] B. Ghanbarian, A.G. Hunt, R.P. Ewing, M. Sahimi, Tortuosity in Porous Media: A Critical Review, Soil Science Society of America Journal. 77 (2013) 1461. https://doi.org/10.2136/sssaj2012.0435.

[6] N. Rey-Raap, J. Angel Menéndez, A. Arenillas, RF xerogels with tailored porosity over the entire nanoscale, Microporous and Mesoporous Materials. 195 (2014) 266–275. https://doi.org/10.1016/j.micromeso.2014.04.048.

[7] N. Rey-Raap, A. Arenillas, J.A. Menéndez, A visual validation of the combined effect of pH and dilution on the porosity of carbon xerogels, Microporous and Mesoporous Materials. 223 (2016) 89–93. https://doi.org/10.1016/j.micromeso.2015.10.044.

[8] I.D. Alonso-Buenaposada, N. Rey-Raap, E.G. Calvo, J. Angel Menéndez, A. Arenillas, Effect of methanol content in commercial formaldehyde solutions on the porosity of RF carbon xerogels, Journal of Non-Crystalline Solids. 426 (2015) 13–18. https://doi.org/10.1016/j.jnoncrysol.2015.06.017.

[9] N. Rey-Raap, J. Angel Menendez, A. Arenillas, Simultaneous adjustment of the main chemical variables to fine-tune the porosity of carbon xerogels, Carbon. 78 (2014) 490–499. https://doi.org/10.1016/j.carbon.2014.07.030.

[10] S. Assouline, D. Or, Air entry-based characteristic length for estimation of permeability of variably compacted earth materials: PERMEABILITY OF VARIABLY-COMPACTED EARTH, Water Resources Research. 44 (2008). https://doi.org/10.1029/2008WR006937.

[11] M. Letellier, C. Delgado-Sanchez, M. Khelifa, V. Fierro, A. Celzard, Mechanical properties of model vitreous carbon foams, Carbon. 116 (2017) 562–571. https://doi.org/10.1016/j.carbon.2017.02.020.

[12] Handoyo, F. Fatkhan, F. Del, Digital Rock Physics Aplications: Visualisation Complex Pore and Porosity-Permeability Estimations of the Porous Sandstone Reservoir, in: 2018. https://doi.org/10.1088/1755-1315/132/1/012002.

[13] C.F. Berg, Permeability Description by Characteristic Length, Tortuosity, Constriction and Porosity, Transport in Porous Media. 103 (2014) 381–400. https://doi.org/10.1007/s11242-014-0307-6.

[14] S. Lowell, J.E. Shields, M.A. Thomas, M. Thommes, Characterization of Porous Solids and Powders: Surface Area, Pore Size and Density, Springer Netherlands, Dordrecht, 2004. https://doi.org/10.1007/978-1-4020-2303-3.

[15] A. Celzard, J. Mareche, G. Furdin, Modelling of exfoliated graphite, Progress in Materials Science. 50 (2005) 93–179. https://doi.org/10.1016/j.pmatsci.2004.01.001.

[16] F.-M. Kong, J.D. LeMay, S.S. Hulsey, C.T. Alviso, R.W. Pekala, Gas permeability of carbon aerogels, Journal of Materials Research. 8 (1993) 3100–3105. https://doi.org/10.1557/JMR.1993.3100.

[17] S. Roy, R. Raju, H.F. Chuang, B.A. Cruden, M. Meyyappan, Modeling gas flow through microchannels and nanopores, Journal of Applied Physics. 93 (2003) 4870–4879. https://doi.org/10.1063/1.1559936.
[18] N.T. Burdine, Relative Permeability Calculations From Pore Size Distribution Data, Journal of Petroleum Technology. 5 (1953) 71–78. https://doi.org/10.2118/225-G.
[19] E.M. Cliffel, W.E. Smith, A.D. Schwope, Theory and Applications of Controlled Permeability, in: H.H. Hausner (Ed.), Modern Developments in Powder Metallurgy: Volume 3 Development and Future Prospects, Springer US, Boston, MA, 1966: pp. 114–128. https://doi.org/10.1007/978-1-4684-7712-2_9.
[20] B. Abdelmalek, Z.T. Karpyn, S. Liu, H. Yoon, T. Dewers, Gas permeability measurements from pressure pulse decay laboratory data using pseudo-pressure and pseudo-time transformations, Journal of Petroleum Exploration and Production Technology. 8 (2018) 839–847. https://doi.org/10.1007/s13202-017-0376-5.
[21] F. Rashid, P.W.J. Glover, P. Lorinczi, D. Hussein, R. Collier, J. Lawrence, Permeability prediction in tight carbonate rocks using capillary pressure measurements, Marine and Petroleum Geology. 68 (2015) 536–550. https://doi.org/10.1016/j.marpetgeo.2015.10.005.
[22] B. Xiao, W. Wang, X. Zhang, G. Long, J. Fan, H. Chen, L. Deng, A novel fractal solution for permeability and Kozeny-Carman constant of fibrous porous media made up of solid particles and porous fibers, Powder Technology. 349 (2019) 92–98. https://doi.org/10.1016/j.powtec.2019.03.028.
[23] R. Lenormand, C. Zarcone, Capillary fingering: Percolation and fractal dimension, Transport in Porous Media. 4 (1989). https://doi.org/10.1007/BF00223630.
[24] C.A. León y León, New perspectives in mercury porosimetry, Advances in Colloid and Interface Science. 76–77 (1998) 341–372. https://doi.org/10.1016/S0001-8686(98)00052-9.
[25] P.A. Webb, An Introduction To The Physical Characterization of Materials by Mercury Intrusion Porosimetry with Emphasis On Reduction And Presentation of Experimental Data, Micromeritics Instrument Corp, Georgia, 2001.
[26] Z. Gao, Q. Hu, Estimating permeability using median pore-throat radius obtained from mercury intrusion porosimetry, Journal of Geophysics and Engineering. 10 (2013) 025014. https://doi.org/10.1088/1742-2132/10/2/025014.
[27] X. Chen, G. Yao, An improved model for permeability estimation in low permeable porous media based on fractal geometry and modified Hagen-Poiseuille flow, Fuel. 210 (2017) 748–757. https://doi.org/10.1016/j.fuel.2017.08.101.
[28] A.J. Katz, A.H. Thompson, Prediction of rock electrical conductivity from mercury injection measurements, Journal of Geophysical Research. 92 (1987) 599. https://doi.org/10.1029/JB092iB01p00599.
[29] A. Celzard, J.F. Marêché, Permeability and formation factor in compressed expanded graphite, J. Phys.: Condens. Matter. 13 (2001) 4387–4403. https://doi.org/10.1088/0953-8984/13/20/302.
[30] G.P. Matthews, C.F. Canonville, A.K. Moss, Use of a void network model to correlate porosity, mercury porosimetry, thin section, absolute permeability, and NMR relaxation time data for sandstone rocks, Physical Review E. 73 (2006) 031307. https://doi.org/10.1103/PhysRevE.73.031307.
[31] H. Ma, Mercury intrusion porosimetry in concrete technology: tips in measurement, pore structure parameter acquisition and application, Journal of Porous Materials. 21 (2014) 207–215. https://doi.org/10.1007/s10934-013-9765-4.
[32] S. Zhou, D. Liu, Y. Cai, Y. Yao, Z. Li, 3D characterization and quantitative evaluation of pore-fracture networks of two Chinese coals using FIB-SEM tomography, International Journal of Coal Geology. 174 (2017) 41–54. https://doi.org/10.1016/j.coal.2017.03.008.
[33] S. Carniglia, Construction of the tortuosity factor from porosimetry, Journal of Catalysis. 102 (1986) 401–418. https://doi.org/10.1016/0021-9517(86)90176-4.
[34] S.K. Datta, N. Simhai, S.N. Tewari, M. Singh, Permeability of microporous carbon preforms, Metallurgical and Materials Transactions A. 27 (1996) 3669–3674. https://doi.org/10.1007/BF02595458.
[35] S. Mauran, L. Rigaud, O. Coudevylle, Application of the Carman–Kozeny Correlation to a High-Porosity and Anisotropic Consolidated Medium: The Compressed Expanded Natural Graphite, Transport in Porous Media. 43 (2001) 355–376.
[36] S.M.R. Niya, A.P.S. Selvadurai, A Statistical Correlation Between Permeability, Porosity, Tortuosity and Conductance, Transport in Porous Media. 121 (2018) 741–752. https://doi.org/10.1007/s11242-017-0983-0.
[37] C.M. Gribble, G.P. Matthews, G.M. Laudone, A. Turner, C.J. Ridgway, J. Schoelkopf, P.A.C. Gane, Porometry, porosimetry, image analysis and void network modelling in the study of the pore-level

properties of filters, Chemical Engineering Science. 66 (2011) 3701–3709. https://doi.org/10.1016/j.ces.2011.05.013.
[38] C. Lin, J.A. Ritter, Effect of synthesis pH on the structure of carbon xerogels, Carbon. 35 (1997) 1271–1278. https://doi.org/10.1016/S0008-6223(97)00069-9.
[39] A. Arenillas, A.H. Moreno, E.G. Calvo, N. Rey-Raap, J.A. Menéndez, Microwave-induced synthesis and curing of RF-polymers, 14th International Conference on Microwave and High Frequency Heating. United Kingdom (2013) 151–154.
[40] J. Hager, M. Hermansson, R. Wimmerstedt, Modelling steam drying of a single porous ceramic sphere: experiments and simulations, Chemical Engineering Science. 52 (1997) 1253–1264. https://doi.org/10.1016/S0009-2509(96)00493-9.
[41] D.S. Springer, H.A. Loaiciga, S.J. Cullen, L.G. Everett, Air permeability of porous materials under controlled laboratory conditions, Groundwater. 36 (1998) 558–565. https://doi.org/10.1111/j.1745-6584.1998.tb02829.x.
[42] M. Thommes, K. Kaneko, A.V. Neimark, J.P. Olivier, F. Rodriguez-Reinoso, J. Rouquerol, K.S.W. Sing, Physisorption of gases, with special reference to the evaluation of surface area and pore size distribution (IUPAC Technical Report), Pure and Applied Chemistry. 87 (2015). https://doi.org/10.1515/pac-2014-1117.
[43] L. Zubizarreta, A. Arenillas, J.A. Menéndez, J.J. Pis, J.-P. Pirard, N. Job, Microwave drying as an effective method to obtain porous carbon xerogels, Journal of Non-Crystalline Solids. 354 (2008) 4024–4026. https://doi.org/10.1016/j.jnoncrysol.2008.06.003.
[44] N. Job, R. Pirard, J. Marien, J.-P. Pirard, Porous carbon xerogels with texture tailored by pH control during sol–gel process, Carbon. 42 (2004) 619–628. https://doi.org/10.1016/j.carbon.2003.12.072.
[45] H. Tamon, H. Ishizaka, T. Araki, M. Okazaki, Control of mesoporous structure of organic and carbon aerogels, Carbon. 36 (1998) 1257–1262. https://doi.org/10.1016/S0008-6223(97)00202-9.
[46] A.M. ElKhatat, S.A. Al-Muhtaseb, Advances in Tailoring Resorcinol-Formaldehyde Organic and Carbon Gels, Advanced Materials. 23 (2011) 2887–2903. https://doi.org/10.1002/adma.201100283.
[47] I.D. Alonso-Buenaposada, N. Rey-Raap, E.G. Calvo, J.A. Menéndez, A. Arenillas, Acid-based resorcinol-formaldehyde xerogels synthesized by microwave heating, Journal of Sol-Gel Science and Technology. 84 (2017) 60–69. https://doi.org/10.1007/s10971-017-4475-z.
[48] M. Firouzi, K. Alnoaimi, A. Kovscek, J. Wilcox, Klinkenberg effect on predicting and measuring helium permeability in gas shales, International Journal of Coal Geology. 123 (2014) 62–68. https://doi.org/10.1016/j.coal.2013.09.006.
[49] A.F. Miguel, A. Serrenho, On the experimental evaluation of permeability in porous media using a gas flow method, Journal of Physics D: Applied Physics. 40 (2007) 6824–6828. https://doi.org/10.1088/0022-3727/40/21/050.
[50] S. Biloe, S. Mauran, Gas flow through highly porous graphite matrices, Carbon. 41 (2003) 525–537. https://doi.org/10.1016/S0008-6223(02)00363-9.
[51] M. Yoshimune, T. Yamamoto, M. Nakaiwa, K. Haraya, Preparation of highly mesoporous carbon membranes via a sol-gel process using resorcinol and formaldehyde, Carbon. 46 (2008) 1031–1036. https://doi.org/10.1016/j.carbon.2008.03.007.
[52] A. Demilecamps, M. Alves, A. Rigacci, G. Reichenauer, T. Budtova, Nanostructured interpenetrated organic-inorganic aerogels with thermal superinsulating properties, Journal of Non-Crystalline Solids. 452 (2016) 259–265. https://doi.org/10.1016/j.jnoncrysol.2016.09.003.
[53] B. Karakashov, J. Toutain, F. Achchaq, P. Legros, V. Fierro, A. Celzard, Permeability of fibrous carbon materials, Journal of Materials Science. 54 (2019) 13537–13556. https://doi.org/10.1007/s10853-019-03854-5.
[54] J. González-García, P. Bonete, E. Expósito, V. Montiel, A. Aldaz, R. Torregrosa-Maciá, Characterization of a carbon felt electrode: structural and physical properties, Journal of Materials Chemistry. 9 (1999) 419–426. https://doi.org/10.1039/a805823g.
[55] G.S. Armatas, Determination of the effects of the pore size distribution and pore connectivity distribution on the pore tortuosity and diffusive transport in model porous networks, Chemical Engineering Science. 61 (2006) 4662–4675. https://doi.org/10.1016/j.ces.2006.02.036.
[56] A. Seifi, A.R. Bahramian, A. Sharif, Correlation between structure and oxidation behavior of carbon aerogels, Journal of Energy Storage. 7 (2016) 195–203. https://doi.org/10.1016/j.est.2016.07.003.

Supplementary Information

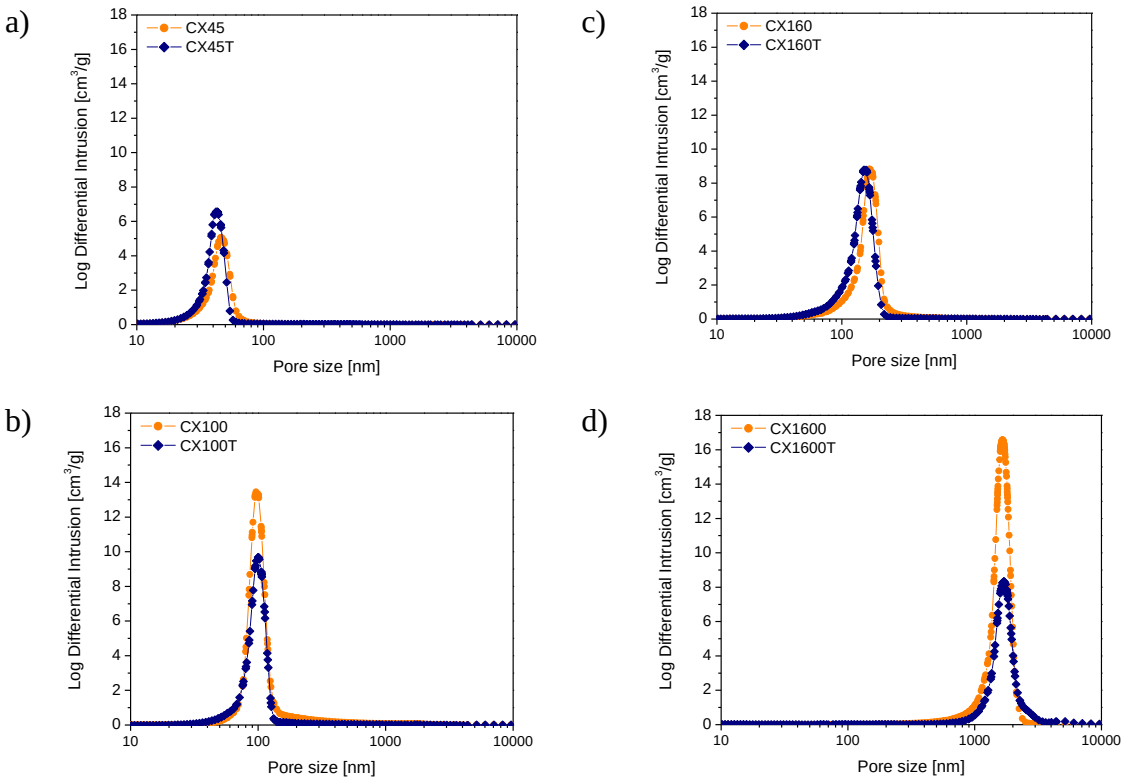

Figure S1. Pore size distribution from Hg intrusion for each pair of samples.

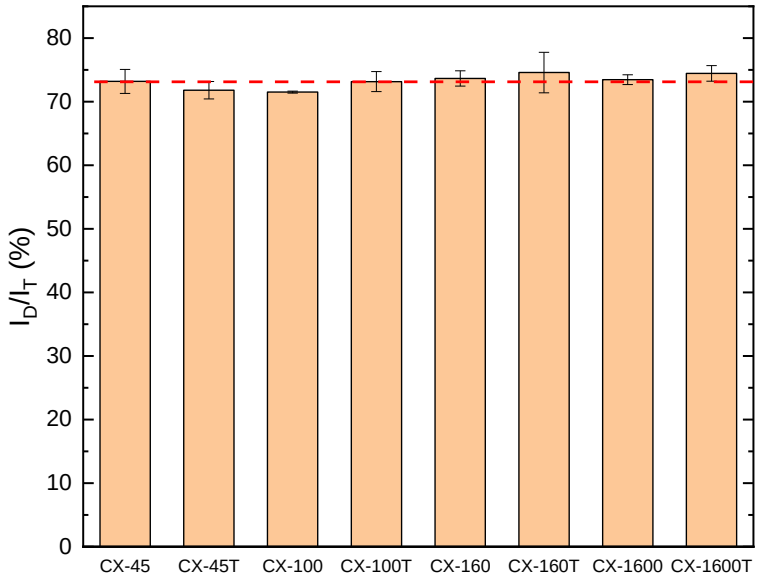

Figure S2. I_D/I_T (%) values of the carbon gels. The red line corresponds to the average value (73.3% ± 1.8%) calculated from all measurements carried out on the CXs.

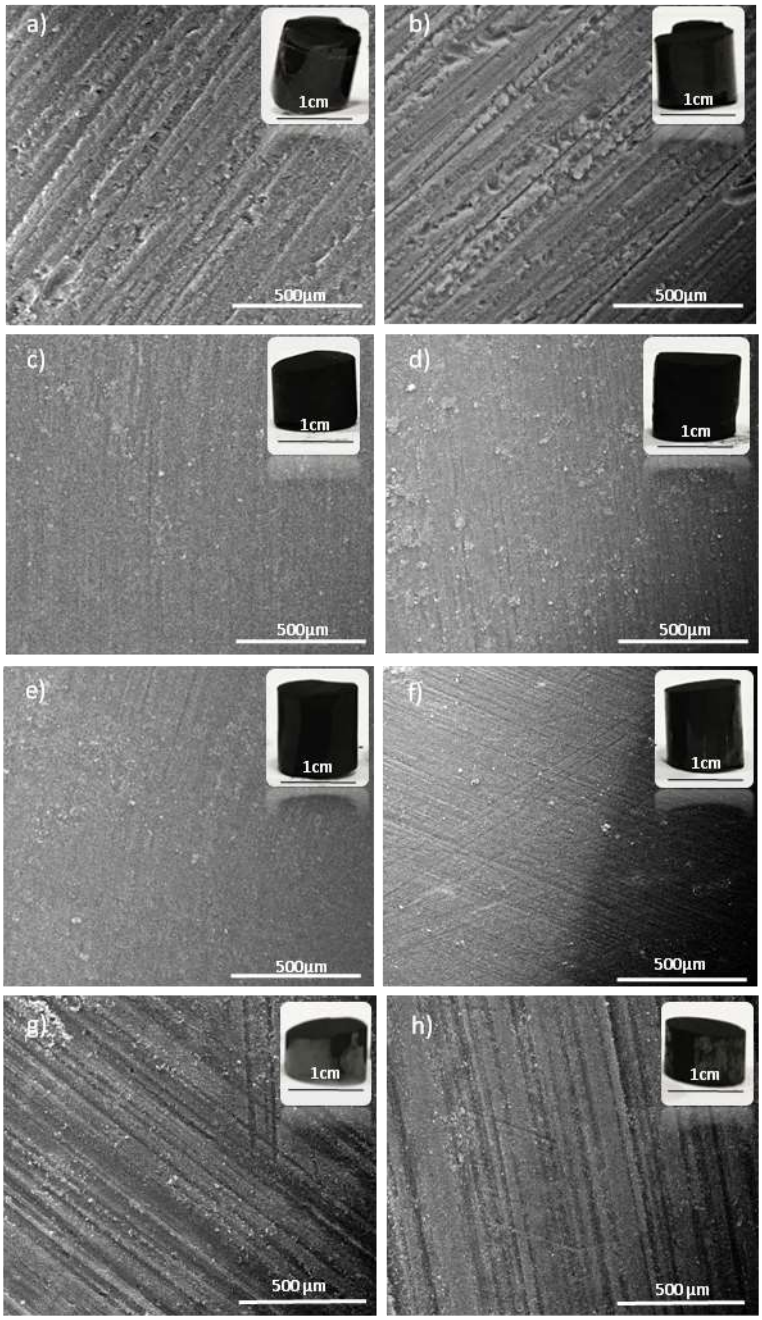

Figure S3. Macroscopic appearance of cylindrical pieces of carbon gels. a) CX-45T, b) CX-45, c) CX-100T, d) CX-100, e) CX-160T, f) CX-160, g) CX-1600T and h) CX-1600.

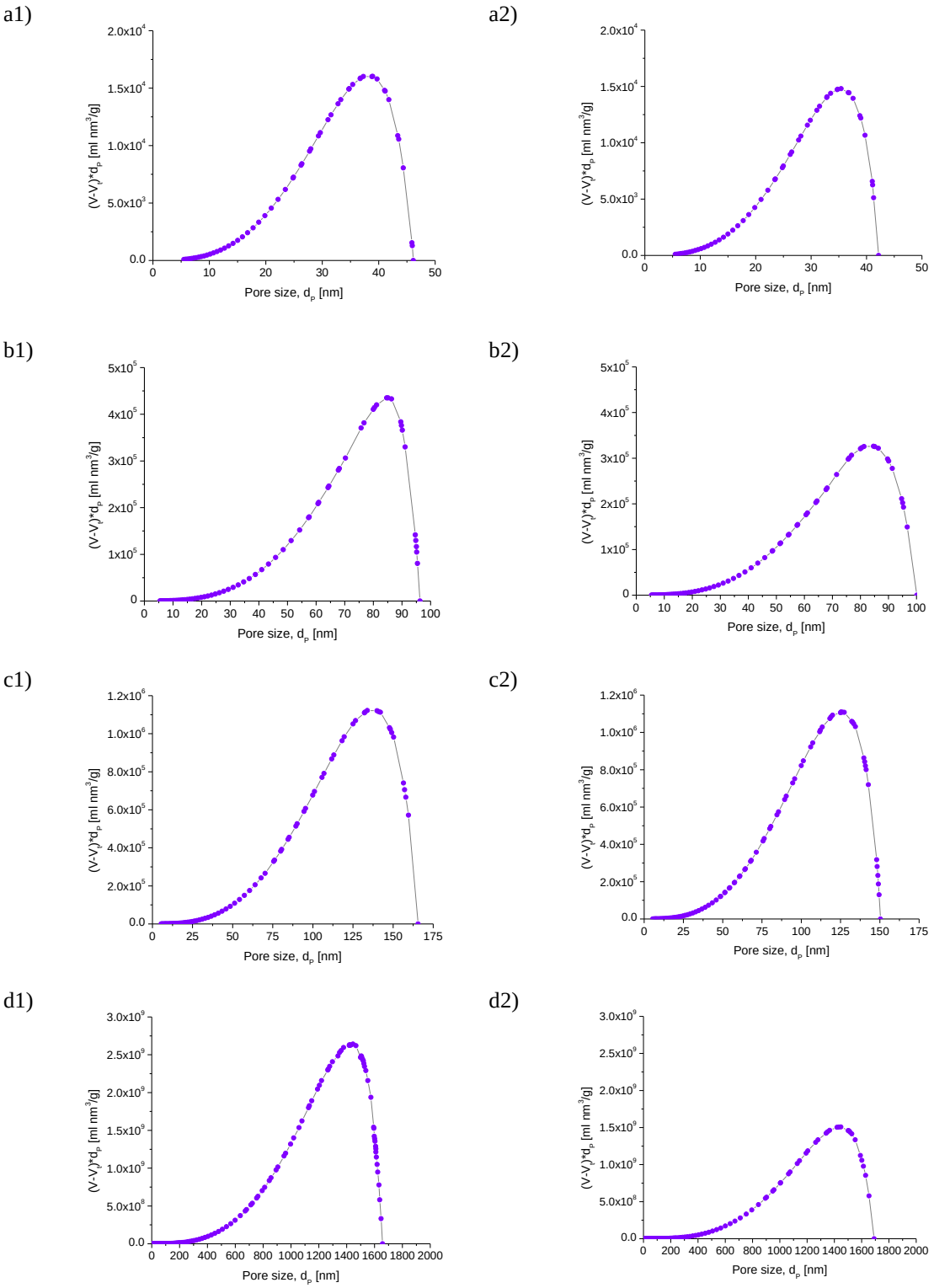

Figure S4. Diffusion path of carbon gels for determination of length of maximum diffusion a1) CX-45, a2) CX-45T, b1) CX-100, b2) CX-100T, c1) CX-160, c2) CX-160T, d1) CX-1600,d2) CX-1600T

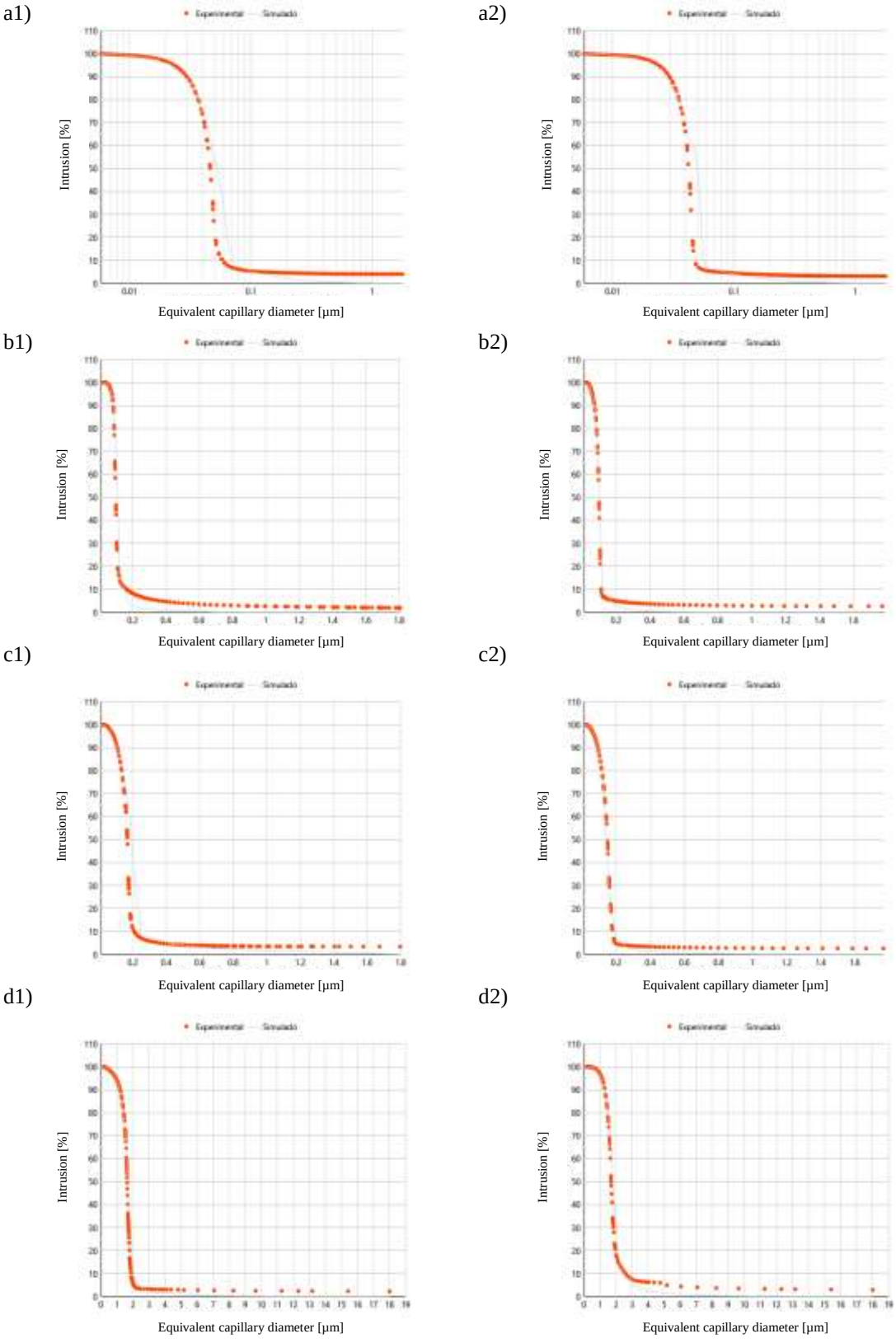

Figure S5. Model fitting used in Pore Xpert to simulate a unit cell from the porosimetry data a1) CX-45 Random, a2) CX-45T Small to large, b1) CX-100 Large to small, b2) CX-100T Random, c1) CX-160 Small to large, c2) CX-160T Random, d1) CX-1600 Random, d2) CX-1600T Large to small

Graphical abstract